PCCP

Accepted Manuscript

ROYAL SOCIETY OF CHEMISTRY

www.rsc.org/pccp

Physical Chemistry Chemical Physics
CREATED USING THE RSC LaTeX PCCP ARTICLE TEMPLATE – SEE www.rsc.org/electronicfiles FOR DETAILS
ARTICLE TYPE www. rsc.org/xxxxxx | XXXXXXXX

Transport in ferrocene single molecules for terahertz applications

G. A. Nemnes*[a] and Adela Nicolaev[a]

Received Xth XXXXXXXXXX 20XX, Accepted Xth XXXXXXXXX 20XX
First published on the web Xth XXXXXXXXXX 200X
DOI: 10.1039/b000000x

The transport properties of single ferrocene molecules connected to nanoscopic gold electrodes are investigated in the framework of density functional theory (DFT) calculations using the non-equilibrium Green's function formalism. Our setup describes a molecular rotor, where one cyclopentadienyl (Cp) ring of the ferrocene molecule is fixed by the two electrodes, while the second ring is able to rotate. For small enough rotation energies the barrier between the eclipsed and staggered conformations of the ferrocene molecule ensures the functionality of a molecular oscillator. The changes in the transmission function introduced by the relative rotation angle between the two Cp rings are analyzed in both linear and non-linear bias regimes. For larger rotation energies, the device works in spinning mode. The real time behavior of the nanomechanical device is investigated using DFT-based molecular dynamics, which shows its feasibility for applications in terahertz regime. In the oscillating mode the natural frequencies are determined, while the spinning mode shows a remarkably reliable behavior with increasing rotation energy.

1 Introduction

Organometallic molecular structures are currently investigated as promising candidates for achieving the ultimate scaling of various electronic devices[1]. Exploiting the unique properties of organic molecules a wide range of applications have been devised, among which one can mention molecular transistors[2,3], current rectifiers[4–6], spin filters[7] and spin current switches[8] or photochromic switches[9]. Besides the electro-optical properties the mechanical properties are also in the focus of recent studies which concern molecular machines and their components, such as e.g. molecular rotors[10], brakes[11] and motors[12]. Based on conformation dependent conduction properties, molecular electronic oscillators may be designed with typical frequencies in the terahertz regime. This frequency domain, in-between the microwaves and far-infrared, usually termed as terahertz gap[13], is currently under intensive research.

Ferrocene is one example from the broader class of 3*d* metallocenes which posses high chemical and thermal stability[14]. It consists of two cyclopentadienyl (Cp) rings bound by a central iron atom, which may rotate about the Cp-Fe-Cp axis. In the condensed phase the ground state is found to be the staggered configuration (D5d), while in the gas phase it corresponds to the eclipsed configuration (D5h). For the isolated molecule the difference between the staggered and the eclipsed configurations is about ~ 20 meV.

Metal-molecule junctions based on ferrocene molecules have been recently investigated[15], providing insights into absorption, spin configuration and charge redistribution process. Molecular circuits with several ferrocene compounds as active region have been analyzed[16–18], indicating the possibility of fine tuning of the molecular conductance. Furthermore, molecular quantum dot cellular automata for THz operating frequencies in high density device have been investigated[19] and spintronic devices have been proposed by attaching metallocene molecules to carbon nanotubes via transition metal atoms[20].

In this paper we investigate the transport properties of single ferrocene molecules attached to gold nanoscopic electrodes, pointing out the feasibility of the device structure as a terahertz oscillator. In our particular setup, one of the Cp rings can rotate, allowing for distinct couplings to the contacts, which result in current variations. The paper is structured as follows. In the next section, details about the device model, computational method and geometric optimizations are presented. In the following section the ballistic transmission function in both linear and non-linear bias regimes is evaluated for different ferrocene conformations, pointing out the changes that occur due to the relative rotation of the Cp rings. Using molecular dynamics in the framework of DFT, the ferrocene-based molecular system is investigated in both oscillating and spinning regimes, showing that the typical frequencies found are in the range of the terahertz domain.

2 Model and Method

The active element of the molecular device is the ferrocene molecule depicted in Fig. 1 (a) and (b) in the eclipsed and staggered conformations. The ferrocene molecule is attached to nanoscopic gold contacts via a pair of sulfur atoms, which ensure strong binding, as indicated in Fig. 1(c). In this setup,

[a] *University of Bucharest, Faculty of Physics, Materials and Devices for Electronics and Optoelectronics Research Center, P.O. Box MG-11, 077125 Magurele-Ilfov, Romania. Fax: +40 (0)21 457 4418; Tel: +40 (0)21 457 4949/157; E-mail: nemnes@solid.fizica.unibuc.ro.*

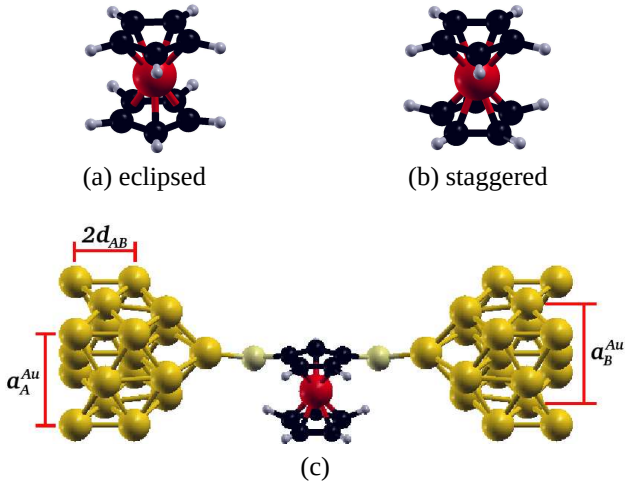

Fig. 1 Ferrocene molecules in the eclipsed (a) and staggered (b) conformations. (c) Nanoscopic Au electrodes are attached via two sulfur atoms. The lattice parameters specifying the relaxed electrode structure are indicated.

one Cp ring of the ferrocene molecule connected to the gold electrodes is fixed, while the other can rotate.

Geometry optimizations are performed using the SIESTA package[21], which takes advantage of the localized basis set of numerical atomic orbitals to achieve linear scaling of the computational time with the system size. The DFT calculations are performed using the local density approximation, in the parametrization proposed by Ceperley and Alder[22]. Structural relaxations are performed using a Monkhorst-Pack scheme of $1 \times 1 \times 10$ k-points, with a maximum force tolerance of 0.04 eV/Å.

Table 1 Optimized structural parameters for different values L_z, for the eclipsed (e) and staggered (s) conformations.

L_z [Å]	d_{Au-S} [Å]	d_{C-S} [Å]	$\alpha_{C-S-Au}[^\circ]$
24(e)	2.95	1.84	150.29
24(s)	2.96	1.85	150.28
23.5(e)	2.58	1.89	146.06
23.5(s)	2.61	1.89	143.98
23(e)	2.47	1.88	140.49
23(s)	2.48	1.87	140.06

First, the Au nanoscopic electrode is investigated, which is a periodic A-B type stacking along the [001] direction of fcc-Au, having 9 atoms per unit cell. Following relaxations, the fcc structure becomes contracted along the transport direction, i.e. the distance between the two layers A and B becomes $d_{AB} = 1.34$Å, which is smaller than half of the bulk lattice constant, $a_0^{Au}/2 = 2.04$Å. Due to the under-coordinated atoms of the atomic sized nanowires, local strain is induced and the bonds become shorter and stronger[23]. The wire is slightly

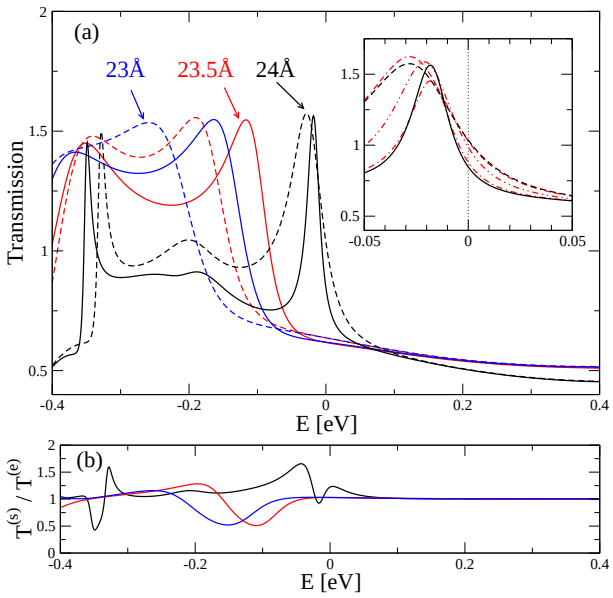

Fig. 2 (a) Transmission vs. energy for the structures with different L_z: 24Å (black), 23.5Å (red), 23Å (blue) for the eclipsed (solid) and staggered (dashed) configurations. The inset contains similar data for the structure with $L_z = 24$Å, for three intermediate rotation angles, $\theta = 8^\circ$ (dot - dashed), 16° (dot - dot - dashed), 28° (dot - dashed - dashed). (b) The ratio of the transmission functions in the two configurations, $T^{(s)}/T^{(e)}$.

expanded in crossection, when compared with the bulk parameter a_0^{Au}. The parameters $a_A^{Au} = 4.76$Å and $a_B^{Au} = 5.18$Å indicated in Fig. 1(c) correspond to the layer of type A and B, respectively.

Having the structural configuration of the semi-infinite electrodes determined, the geometry of the whole system containing the ferrocene molecule is optimized. The structural data is summarized in Table 1. The electrodes are positioned at different distances, denoted by L_z, measuring the distance between the first and the last Au layer depicted in Fig. 1(c). Increasing L_z from 23Å to 24Å, the Au-S bonds are stretched, resulting in larger angles α_{C-S-Au}. The data in Table 1 shows that the Au-S bond changes significantly, while the C-S bond remains largely unaffected, indicating the Au-S bond is comparatively weaker.

3 Results and discussion

3.1 Ballistic transmission

The ballistic transmission is calculated by employing the non-equilibrium Green's functions formalism (NEGF), implemented in TRANSIESTA[24]. Using the advanced/retarded Green's functions $G^{a/r}$ and the self-energies $\Gamma_{L/R}$ describing

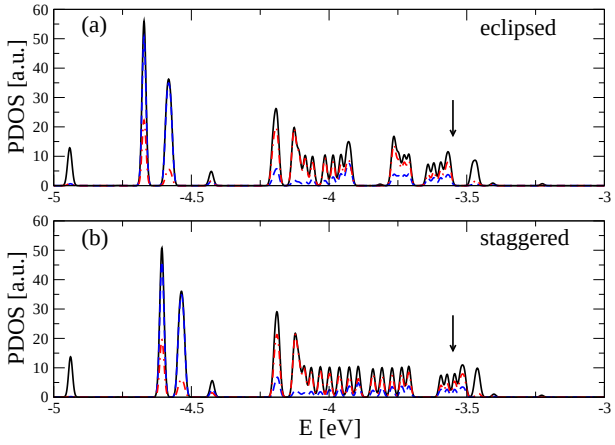

Fig. 3 Partial density of states for the eclipsed (a) and staggered (b) conformations ($L_z = 24$Å), presented for different groups of atoms: C, H, Fe, S (black / solid); C, H, S (red / dot - dashed); C, H, Fe (blue / dashed). The arrows mark the chemical potentials.

the coupling between the molecular system and the contacts, one may write the transmission function as:

$$T(E) = \mathrm{Tr}[\Gamma_{\mathrm{L}}(E) G^r(E) \Gamma_{\mathrm{R}}(E) G^a(E)]. \qquad (1)$$

We first investigate the transport in the linear bias regime. Figure 2(a) shows the transmission functions for three different values L_z, with the ferrocene molecule in the eclipsed and staggered configurations. Decreasing L_z, the peaks in transmission are shifted towards lower energies. This indicates the possibility of controlling the transmission at the Fermi energy ($\mu = 0$), by adjusting the distance between the electrodes. The peaks in transmission become broader as the distance is decreased, due to an enhanced coupling between the molecule system and the contacts. Switching from the eclipsed to the staggered conformation, the peaks also become broader. In the eclipsed configuration the overlapping p-orbitals of pairs of the carbon atoms from equivalent positions in the two Cp rings is stronger than in the staggered conformation. Instead, in the staggered configuration the overlap between the same orbitals and the neighboring sulfur atoms is larger, which is in-line with the observed increased coupling in the transmission function. To show the role of the sulfur atoms in the transmission we plotted in Fig. 3 the partial density of states. The peaks in the vicinity of the chemical potential are dominated by sulfur orbitals and a smaller contribution from the iron atom in the structure of the ferrocene molecule. Detailed analysis of the transmission function at the Fermi energy, as a function of the rotation angle θ shows that the maximum is reached for the staggered configuration. The transmission functions for three intermediate configurations, $\theta = 8^\circ, 16^\circ, 28^\circ$ are depicted in the inset of Fig. 2(a). The change in the conductance is measured as the ratio between the transmission functions

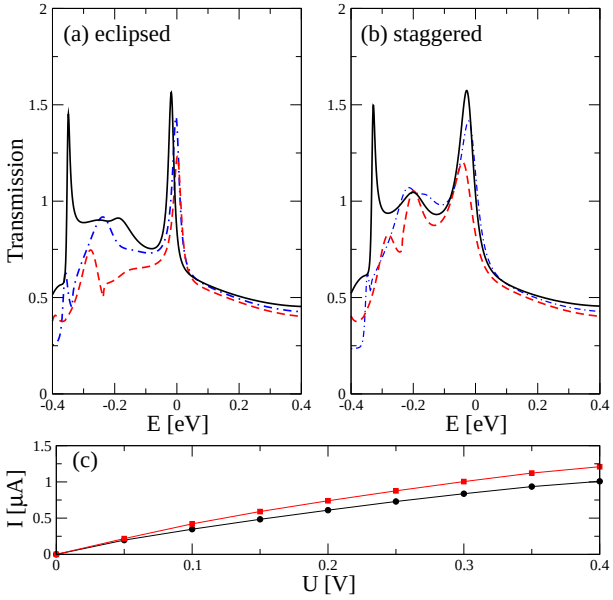

Fig. 4 Transmission vs. energy at finite bias, for the structure with L_z=24Å, in the eclipsed (a) and staggered (b) configurations: $U = 0V$ (black/solid), $U = 0.2V$ (blue/dot-dashed) and $U = 0.4V$ (red/dashed). (c) Current vs. bias for the two configurations, eclipsed (black/circles) and staggered (red/squares).

in the staggered and eclipsed configurations. For $L_z = 24$Å one obtains a ratio $T^{(s)}/T^{(e)} = 1.22$, which can be exploited in signal generation.

3.2 Non-linear bias regime

We also investigate the non-linear bias regime. The current is calculated for a bias U up to 0.4V in steps of 0.05V. The transmission functions are plotted in Fig. 4(a) and (b) for the two conformations. The general trend observed is a decrease in the transmission function with the applied bias, due to the asymmetry induced by the applied electric field which enhances the elastic scattering. Figure 4(c) shows the current vs. applied bias calculated within the coherent transport formalism with the relation:

$$I = \frac{2e}{h} \int dE\; T(E;U)\; [f_{\mathrm{FD}}(E;\mu_{\mathrm{L}}) - f_{\mathrm{FD}}(E;\mu_{\mathrm{R}})], \qquad (2)$$

where $\mu_{\mathrm{L}} = eU/2$ and $\mu_{\mathrm{R}} = -eU/2$ are the chemical potentials in the left and right contacts, respectively. The staggered configuration ensures a better coupling with the contacts than the eclipsed configuration and therefore the lifetime of the resonances is decreased. As a consequence the current obtained for the staggered conformation is ∼20% larger at the maximum bias considered $U = 0.4$ V. Ferrocene-based molecular wires[25] have been investigated experimentally in the non-linear bias regime, recently by using the STM break junc-

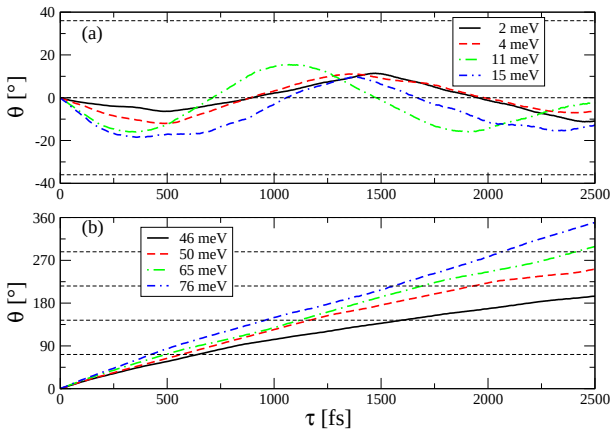

Fig. 5 Rotation angle of the Cp ring vs. time, for the oscillating mode (a) and for the spinning mode (b). The horizontal dashed lines mark the range of the rotation angle, +/-36° (a) and, in steps of 72°, the equivalent positions, in this case the eclipsed conformations (b).

tion technique[26] and different anchoring groups to contact the electrodes to each of the two Cp rings.

3.3 Molecular dynamics

In the case of pristine ferrocene molecules, there is a rotational energy barrier E_b with respect to the metal-cyclopentadienyl axis of ∼2kJ/mol (∼ 20.7 meV)[27], which is comparable with other DFT calculations[28] and with experimental data measured by gas phase electron diffraction[29].

We perform molecular dynamics calculations using the Verlet algorithm. Depending on the rotation energy, E_0, imposed on the second Cp ring, assuming the ferrocene molecule initially in the eclipsed configuration, one can distinguish between two regimes. For $E_0 < E_b$, i.e. the low energy regime, the Cp ring oscillates with a maximum dihedral angle below 36°, which corresponds to the staggered conformation. Figure 5(a) shows the dynamics of the Cp ring, in the low energy regime, measured by the dihedral angle θ, for a time interval $\tau = 2.5$ ps. One can see that for the 2-4 meV range, the oscillation period is ∼1 ps. One period is defined by time to reach an equivalent conformation. By increasing the rotation energy to 11 meV, the amplitude is getting larger, i.e. $\theta_{max} \approx 16°$, and the period decreases to ∼0.72 ps. However, increasing further the rotation energy the systems spends more time at the point where the rotation is reversed. Consequently, the oscillation period is getting larger. Part of the initial kinetic energy is transferred to neighboring atoms and in-between the C and H atoms of the rotating Cp ring. Near the critical point $E_0 = E_b$, which corresponds to a complete stop in the staggered conformation, the oscillations become unstable.

A more predictable behavior is obtained for larger rotation energies, above E_b. In this case, the Cp ring rotates continuously and the molecule is passing successively through the staggered and eclipsed configurations. By increasing the rotation energy, the periods are systematically smaller, ranging from 0.65 ps for 46 meV to 0.42 ps for 76 meV, as indicated in Fig. 5(b). One should also note that the angular velocity is slightly decreasing in time for lower energies, due to the fact that a larger fraction of the kinetic energy is transferred. However, increasing the rotation energy of the Cp ring, the system becomes more stable.

The rotation of the Cp ring in the context of varying transmission function with the angle θ is the prerequisite for the device to work as a signal generator. The operating frequencies are found in the range of 1-1.4 THz for the oscillating mode, which are natural frequencies of the system and 1.5-2.4 THz for the spinning mode. The device structure is therefore suitable for applications in the terahertz regime.

4 Conclusions

We investigate a ferrocene based molecular device in the framework of density functional theory calculations. In our setup one cyclopentadienyl ring is connected to nanoscopic gold electrodes, while the other one can rotate, indicating the possibility of producing electrical signals in the terahertz regime. We analyzed in detail the structural features and the coupling between the contacts and the molecular systems in the context of adjusting the distance between the electrodes. Both linear and non-linear bias regimes have been considered and the results indicated a significant difference between the eclipsed and staggered conformations of the ferrocene molecule, in the context of coupling to the electrodes. We employed molecular dynamics calculations within the DFT approach and determined the nanomechanical properties. We distinguished between two regimes, the oscillation regime for low rotation energies generated by the internal rotation barrier and the spinning regime, for large rotation energies. The natural frequencies of the Cp ring oscillations were established as a function of rotation energy and the stability of current variations was discussed. To conclude, we indicate the possibility of using a rotating molecular device with the ferrocene molecule as active element for terahertz applications.

References

1 *Conducting and Magnetic Organometallic Molecular Materials*, ed. L. O. M. Fourmigue, Springer, Berlin/Heidelberg, 2009.
2 H. Song, Y. Kim, Y. H. Jang, H. Jeong, M. A. Reed and T. Lee, *Nature*, 2009, **462**, 1039.
3 K. Sotthewes, V. Geskin, R. Heimbuch, A. K. and H. J. W. Zandvliet, *APL Mat.*, 2014, **2**, 010701.
4 G. J. Ashwell, R. Hamilton and L. R. H. High, *J. Mater. Chem.*, 2003, **13**, 1501.

5 N. J. Geddes, J. R. Sambles and A. S. Martin, *Adv. Mater. Optic. Electron.*, 2004, **5**, 305.
6 F. Ding, S. Chen and H. Wang, *Materials*, 2010, **3**, 2668.
7 S. Sanvito, *Nature Materials*, 2011, **10**, 484.
8 Y. Ni, K. lun Yao, C. qun Tang, G. ying Gao, H. hua Fub and S. cong Zhub, *RSC Adv.*, 2014, **4**, 18522.
9 L. Zhu, K. L. Yao and Z. L. Liu, *Appl. Phys. Lett.*, 2010, **97**, 202101.
10 G. S. Kottas, L. I. Clarke, D. Horinek and J. Michl, *Chem. Rev.*, 2005, **105**, 1281.
11 J.-S. Yang, Y.-T. Huang, J.-H. Ho, W.-T. Sun, H.-H. Huang, Y.-C. Lin, S.-J. Huang, S.-L. Huang, H.-F. Lu and I. Chao, *Org. Lett.*, 2008, **10**, 2279.
12 J. Michl and E. C. H. Sykes, *ACS Nano*, 2009, **3**, 1042.
13 P. H. Siegel, *IEEE Transactions on Microwave Theory*, 2002, **50**, 910.
14 C. Engtrakul and L. R. Sita, *Nano Lett.*, 2001, **1**, 541.
15 D. M. Djimbi, S. L. Roux, C. Massobrio and M. Boero, *J. Phys.: Condens. Matter.*, 2014, **26**, 104206.
16 T. Uehara, R. V. Belosludov, A. A. Farajian, H. M. Izuseki and Y. Kawazoe, *Jap. J. Appl. Phys.*, 2006, **45**, 3768.
17 H. Mizuseki, R. V. Belosludov, T. Uehara, S. U. Lee and Y. Kawazoe, *J. Kor. Phys. Soc.*, 2008, **52**, 1197.
18 C. Morari, I. Rungger, A. R. Rocha, S. Sanvito, S. Melinte and G.-M. Rignanese, *ACS NANO*, 2009, **3**, 4137.
19 V. Cauda, M. Graziano, D. Demarchi, G. Piccinini, A. Sanginario and A. Pulimeno, *IEEE Transactions on Nanotechnology*, 2013, **12**, 498.
20 P. Wei, L. Sun, E. Benassi, Z. Shen, S. Sanvito and S. Hou, *J. Chem. Phys.*, 2011, **134**, 244704.
21 J. Soler, E. Artacho, J. Gale, A. Garcia, J. Junquera and D. S.-P. P. Ordejon, *J. Phys.: Condens. Matter*, 2002, **14**, 2745.
22 D. Ceperley and B. Alder, *Phys. Rev. Lett.*, 1980, **45**, 566.
23 X. Zhang, J. lai Kuo, M. Gu, X. Fan, P. Bai, Q.-G. Songe and C. Q. Sun, *Nanoscale*, 2010, **2**, 412.
24 M. Brandbyge, J.-L. Mozos, P. Ordejon, J. Taylor and K. Stokbro, *Phys. Rev. B*, 2002, **65**, 165401.
25 S. A. Getty, C. Engtrakul, L. Wang, R. Liu, S.-H. Ke, H. U. Baranger, W. Yang, M. S. Fuhrer and L. R. Sita, *Phys. Rev. B*, 2005, **71**, 241401(R).
26 Y.-Y. Sun, Z.-L. Peng, R. Hou, J.-H. Liang, J.-F. Zheng, X.-Y. Zhou, X.-S. Zhou, S. Jin, Z.-J. Niua and B.-W. Mao, *Phys. Chem. Chem. Phys.*, 2014, **16**, 2260.
27 N. Mohammadi, A. Ganesan, C. T. Chantler and F. Wang, *J. Organomet. Chem.*, 2012, **713**, 51.
28 S. Coriania, A. Haalanda, T. Helgaker and P. Jorgensen, *Chem. Phys. Chem.*, 2006, **7**, 249.
29 A. Haalanda and J. Nilsson, *Acta Chem. Scand.*, 1968, **22**, 2653.